Quantum Dot Arrays: A New Picture of the Quantum Hall Effect in Two-Dimensional Crystals

Brad L. Johnson and George Kirczenow

Department of Physics, Simon Fraser University, Burnaby, British Columbia, Canada V5A 1S6
(Received 12 March 1992)

We investigate the edge-state spectra of two-dimensional quantum dot arrays (QDA's) in transverse magnetic fields, and the manifestation of the edge states in lateral quantum transport. We show the edge states to be superpositions of normal and counterrotating currents. A Büttiker-Landauer transport analysis of this physical picture predicts positive and negative Hall conductances, quantized in integer and *fractional* multiples of e^2/h, for QDA's connected to ideal reservoirs. The predicted fractions differ in value and origin from the usual fractional quantum Hall effect.

The study of electronic transport in low-dimensional systems has produced many important and fascinating results, both theoretically and experimentally. Of particular interest is the integer quantum Hall effect (IQHE) discovered by von Klitzing, Dorda, and Pepper [1], and the fractional quantum Hall effect (FQHE), first observed by Tsui, Störmer, and Gossard [2]. The IQHE can be understood in terms of a one-particle picture for 2D electrons in transverse magnetic fields. The Hall conductance is quantized in integer multiples of e^2/h when the Fermi energy lies within a band of localized states between Landau levels [3–5]. An alternative point of view, proposed by Streda, Kucera, and MacDonald [6], by Jain and Kivelson [7], and by Büttiker [8], is based on considerations of transport by Halperin's magnetic edge states [4] and the Landauer [9] picture of one-dimensional conduction. The FQHE, on the other hand, is due to electron-electron interactions. The explanation proposed by Laughlin [10] has a ground state which, at specific fractional Landau-level filling factors, becomes an incompressible fluid with fractionally charged excitations. Recent work by Beenakker [11] and by Johnson and MacDonald [12] has also provided a possible edge-state picture of the FQHE.

As was demonstrated by Thouless *et al.* [13] and clarified by Aoki [14], by Rammal *et al.* [15], and by MacDonald [16], the quantum Hall effect should also occur in two-dimensional electron systems in the presence of a periodic potential. Such systems were shown by Azbel [17], by Wannier [18], and by Hofstadter [19] to exhibit a complex fractal one-electron spectrum, the Hofstadter "butterfly." Their Hall conductance has been predicted to be quantized in positive or negative integer multiples of e^2/h when the Fermi level lies in a spectral gap [13–16]. Possible experimental realizations of such systems are two-dimensional electron gases with a weak periodic potential modulation, which have recently been reported by Gerhardts, Weiss, and Wulf [20] to exhibit evidence of the Hofstadter butterfly spectrum, and periodic arrays of quantum dots. Quantum dots are small (~ 1000 Å), few-electron systems formed by lateral confinement of 2D electrons [21–23].

The purpose of this paper is to present a new approach to understanding the quantum Hall effect in periodic arrays of quantum dots in transverse magnetic fields. We will show that, in the context of a one-electron model, the lateral transport problem in these structures is extremely complex: The quantum dot array can support edge currents which "counterrotate," i.e., they exhibit rotation that is opposite to that normally expected from a Lorentz force argument. In some situations, different numbers of both normal and counterrotating edge states exist at the same time. We will show that for particular numbers of normal and counterrotating eigenmodes, it is possible to have integer, negative, and even fractional Hall conductance, i.e., G_H a fraction of e^2/h, in these structures. This represents the first instance of fractional Hall conductance in a one-electron model, with a different physical origin (and different fractions) from the FQHE in 2D electron gases.

To understand the nature of the transport problem in the presence of the array, we consider the following picture. We connect reservoirs to each side of the array as shown schematically in Fig. 1. In this case, one may calculate the Hall conductance G_H from the Büttiker [24] equations $I_j = (K_j\mu_j - \sum_k T_{jk}\mu_k)e/h$, where I_j is the net current injected at reservoir j, K_j is the number of channels injected by reservoir j at the Fermi energy, μ_j is the chemical potential of reservoir j, and T_{jk} is the transmission probability from reservoir k to reservoir j. Now we assume that the reservoirs are ideal, that is, they are perfectly emitting and absorbing. Therefore, edge modes injected from reservoir 1 are completely absorbed into reservoirs 2 and 4, while none are transmitted to 3, and so on for each reservoir. If we denote the number of injected modes circulating in a clockwise sense by N, and those circulating counterclockwise by M (see Fig. 1), we have the following simplifications: $T_{21} = N$, $T_{41} = M$, and $K_1 = N + M$. Applying these relationships in the Büttiker equations, with $I_1 = -I_3 = I$, $I_2 = I_4 = 0$, we find for the Hall conductance

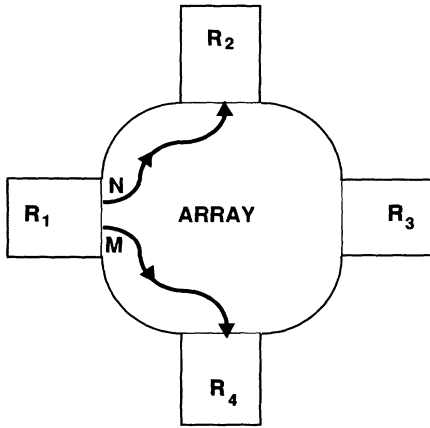$$G_H \equiv \frac{I_e}{\mu_2 - \mu_4} = \frac{e^2}{h}\frac{N^2 + M^2}{N - M}. \tag{1}$$

FIG. 1. Schematic of the quantum dot array attached to ideal reservoirs. The reservoirs are labeled $R1$-$R4$. N normal modes are populated by reservoir 1 and absorbed by reservoir 2, and M counterrotating modes are populated by $R1$ and absorbed at $R4$.

We stress that Eq. (1) applies in the ballistic regime—N and M are independent channels. If the rotating and counterrotating channels are allowed to mix and equilibrate, then Eq. (1) reduces [25] to $G_H = e^2/h(N-M)$ (algebraically summing the edge states), which agrees with the results of Thouless et al. and MacDonald.

From Eq. (1) it follows that a variety of situations are possible: G_H can be positive or negative $(N < M)$, and integer or fractional multiples of e^2/h. The lowest-order fraction is given by $N=4$, $M=1$, i.e., the presence of four clockwise states and one counterclockwise state gives a Hall conductance of $G_H = (e^2/h) \frac{17}{3}$. With this in mind, we now examine the eigenspectrum of the quantum dot array to find the types of solutions (combinations of modes) that should occur in the physical transport problem.

We adopt a model based upon a 2D array of quantum dots connected by narrow constrictions. The geometry of a portion of the array is shown in Fig. 2(a). If the applied magnetic field points along $+z$, then the vector potential may be written in the Landau gauge $\mathbf{A} = (-By,0,0)$. In this gauge, the Hamiltonian of the system is periodic in the x direction, and the eigenstates of the array may be constructed of states in columns of dots via Bloch's theorem. We assume that the individual quantum dots have azimuthal symmetry. The one-electron eigenstates of the individual dots are then characterized by radial and azimuthal quantum numbers n and l, respectively, where n is an integer and the symmetry-breaking effect of the constrictions makes l a continuous variable for open systems [26]. Explicitly, in an arbitrary dot,

$$\Psi(x,y) = e^{ie\pi B(xy_0 - yx_0 + xy)/h} R_n(r-r_0)e^{il\phi} \qquad (2)$$

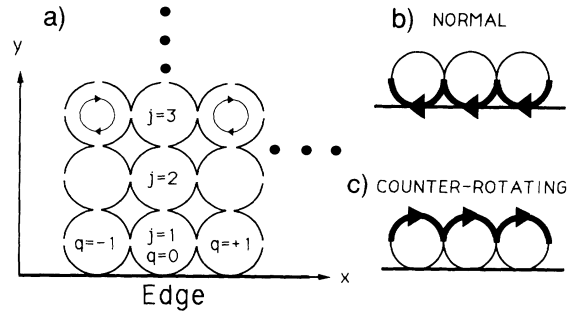where $r_0 = (x_0,y_0)$ is the location of the center of the dot

FIG. 2. (a) Part of the quantum dot array under consideration. The integer q labels the columns of the array, while j labels the dot within a column. The direction of normal electron rotation is given for a magnetic field along $+z$. Illustrations of the simplest (b) normal and (c) counterrotating edge current states of the array [only the dots bordering the edge of the array are shown in (b) and (c)].

and ϕ is the azimuthal angle with respect to the center of the dot.

In what follows, we assume that the external magnetic field is high enough that the individual dots are in the edge-state regime, and therefore only the lowest radial mode need be considered. In this regime, mode mixing occurs only near the constrictions, where an electron may either scatter into modes in the adjacent dot or remain in the same mode and propagate to the next constriction. In propagating from constriction to constriction, the one-electron wave functions acquire a phase shift which may be found from the dot eigenstates (2). We calculate the eigenstates of the array by exploiting the unitarity of the scattering matrices that relate the current amplitudes entering and leaving the vicinity of the constrictions joining different quantum dots [26,27]. For scattering at any constriction in dot j, this yields

$$J_j^0(q) = \sum_{j',q'} U_j^{j'} J_{j'}^l(q') e^{i(q-q')\xi}. \qquad (3)$$

Here J_j^0 is the current amplitude out of the constriction in dot j, $J_{j'}^l$ is the amplitude incident on the constriction in dot j', U is a unitary scattering matrix, and ξ is the Bloch phase. The sum is over the dot numbers bordering the constriction, and each dot number has a corresponding column number q [cf. Fig. 2(a)]. We find the eigenmodes of the system of equations (3) with real ξ for an infinite strip of dots running parallel to the x axis as shown in Fig. 2(a). The propagating modes (with real ξ) are the edge states of the quantum dot array. These modes are localized at or near the array edge, and decay rapidly into the interior. At particular values of field and angular momentum l there may be several eigensolutions, and the net current amplitude will be a superposition of the individual current amplitudes corresponding to the different values of ξ.

Now we turn to our results. As mentioned previously,

we consider a situation in which only the lowest radial mode is occupied per dot. In this case, the angular momentum is roughly a label for the electron number per dot; a change in l by 1 at the Fermi energy is roughly a change in electron number by 1 per dot (in the spin-polarized regime). At fixed B, the eigenmodes of the system are periodic in l (modulo 1). Also, at fixed l, the eigenmodes of the array are periodic in magnetic field B with period $\Delta B = \Phi_0/d^2$, where Φ_0 is the flux quantum and d is the lattice spacing. Therefore, we work in the convenient variables $\lambda = -l$ and $\beta = B/\Delta B$, both modulo 1. For the matrix U we choose the form $U_j^{j'} = [\delta_{j',j}(1 - p^2)^{1/2} + (1 - \delta_{j',j})p] \exp(i\theta_j^{j'})$, where $\theta_j^{j'}$ is the phase shift for scattering from dot j' to dot j, and p^2 is the probability to scatter into an adjacent dot. In what follows, we choose $p^2 = 0.9$, $\theta_j^{j'} = \pi/2$, and $\theta_j^{j} = 0$, consistent with unitarity.

In Fig. 3, we plot the eigenspectra λ vs β for a third of a period in each. We choose this region because (1) the full period in λ and β is highly symmetric and (2) the regions *most important to the transport problem* (the largest number of rotating states, counterrotating states, and mixtures) occur for $\lambda < 0.3$ and $\beta < 0.3$, and in the symmetric region $\lambda, \beta > 0.7$. The unshaded region marked 0,0, where the notation is given by N,M (number of normal and counterrotating states, respectively), is an insulating gap, that is, a region where no propagating solutions exist [27]. The rest of Fig. 3 is divided into regions characterized by the number of distinct edge states (with
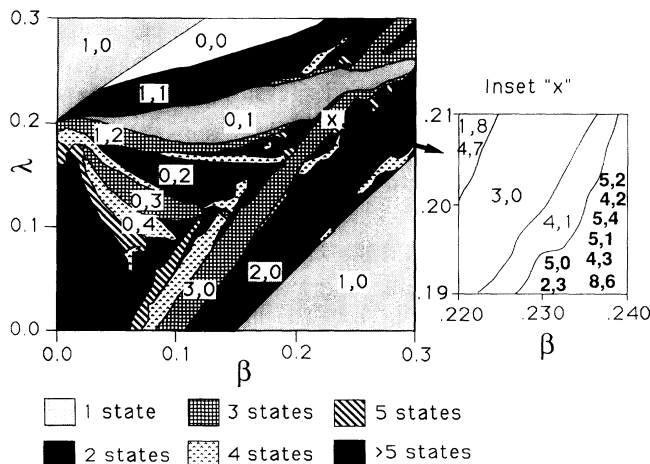
differing real ξ); the light regions have one state, the darker regions have two states, and so on up to five states. Two large one-state regions are marked 1,0. These contain the principal normal edge states, where the current amplitude is predominantly localized at the outermost boundary of the edge dots [see Fig. 2(b)]. Also of interest is the large central one-state region denoted 0,1. This is a region of principal counterrotating edges states—localized predominantly at the *inside* edge of the edge dots, as in Fig. 2(c). Note that for clockwise rotation within an individual dot, a current circulating around the array on only the *inside* portion of the edge dots would have a counterclockwise sense.

Interesting patterns are apparent in Fig. 3. Notice that as one traverses the spectrum from right to left beginning at the principal 1,0 region in the lower right portion of the figure, the number of normal edge states present increases progressively as β is decreased, as long is λ is not too large. In contrast, the effect of mixing normal and counterrotating states causes the progression downward in λ from the principal counterrotating region 0,1 to be irregular; i.e., the sequence from one counterrotating state to two, etc., is interrupted by intermediate regions containing both normal and counterrotating modes. The "buffer" region between the 0,1 region and the 1,0 region in the upper left portion of Fig. 3 is a 1,1 region, as one might expect. The inset corresponds to the region marked "×," and is illustrative of the kind of complexity which exists in the region intermediate between the principal normal and principal counterrotating zones; we note that the complexity here has a different character from the classic Hofstadter spectrum. The states listed explicitly in the inset with > 5 states are only representative, since the character of the eigenstates outside of the 3,0 and 4,1 regions changes on a finer scale than what is shown. In general, note that the region above and to the
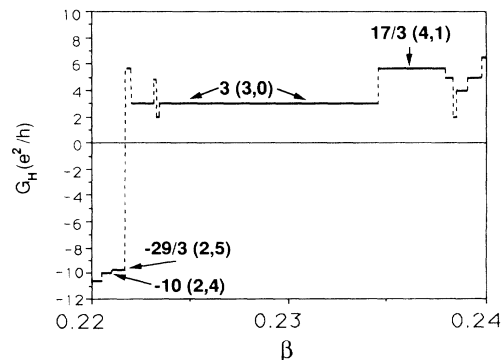
FIG. 3. The eigenspectra of a quantum dot strip with 90% transmission at the constrictions. Here $\lambda = -l$, the dot angular momentum; $\beta = Bd^2/\Phi_0$. The regions are marked according to the total number of propagating edge states as shown, and the labels indicate the number of normal and counterrotating states (N,M). The inset region "×" is enlarged, illustrating the complex region between 0,1 and 1,0 in the spectrum, where there is competition between numbers of rotating and counterrotating states. The labels are representative, and do not constitute all of the distinct regions present in the inset.

FIG. 4. Hall conductance vs β (magnetic field) for fixed $\lambda = 0.206$. See the inset region of Fig. 3. Marked are the integer and fractional plateaus at $G_H = 3$ and $G_H = \frac{17}{3}$, respectively—these correspond to the regions 3,0 and 4,1 in the inset of Fig. 3. Also note the negative plateaus at $G_H = -\frac{29}{3}$ and $G_H = -10$.

left of the 3,0 zone in the inset is dominated by counter-rotating states, while the region below the 4,1 zone is dominated by normal states.

To illustrate the effect of the eigenspectra of the array on transport, Fig. 4 is a plot of Hall conductance [from Eq. (2)] as a function of β for $\lambda = 0.206$—this corresponds to the region of the inset of Fig. 3. We note the presence of an integer plateau at $G_H = 3$, and a fractional plateau at $G_H = \frac{17}{3}$ (the lowest-order fraction), corresponding to the 3,0 and the 4,1 regions of Fig. 3, respectively. In addition, note the negative plateaus in the lower left, corresponding to 2,5 and 2,4 regions, as indicated in the figure.

In conclusion, we have presented an edge-current analysis of the Hall effect in quantum dot arrays that predicts integer, negative, and also novel fractional quantized Hall conductances in a one-electron picture. We have demonstrated that a plausible model of the quantum dot arrays exhibits a rich spectrum of coexisting normal and counterrotating modes, including states that support the predicted fractional Hall conductances.

[1] K. von Klitzing, G. Dorda, and M. Pepper, Phys. Rev. Lett. **45**, 494 (1980).

[2] D. C. Tsui, H. L. Störmer, and A. C. Gossard, Phys. Rev. Lett. **48**, 1559 (1982).

[3] R. B. Laughlin, Phys. Rev. B **23**, 5632 (1981).

[4] B. I. Halperin, Phys. Rev. B **25**, 2185 (1982).

[5] For a review, see *The Quantum Hall Effect*, edited by R.

[6] P. Streda, J. Kucera, and A. H. MacDonald, Phys. Rev. Lett. **59**, 1973 (1987).

[7] J. K. Jain and S. A. Kivelson, Phys. Rev. Lett. **60**, 1542 (1988).

[8] M. Büttiker, Phys. Rev. B **38**, 9375 (1988).

[9] R. Landauer, IBM J. Res. Dev. **1**, 223 (1957).

[10] R. B. Laughlin, Phys. Rev. Lett. **50**, 1395 (1983).

[11] C. W. J. Beenakker, Phys. Rev. Lett. **64**, 216 (1990).

[12] M. D. Johnson and A. H. MacDonald, Phys. Rev. Lett. **67**, 2060 (1991).

[13] D. J. Thouless, M. Kohmoto, M. P. Nightingale, and M. den Nijs, Phys. Rev. Lett. **49**, 405 (1982).

[14] H. Aoki, Phys. Rev. Lett. **55**, 1136 (1985).

[15] R. Rammel, G. Toulouse, M. T. Jackel, and B. I. Halperin, Phys. Rev. B **27**, 5142 (1983).

[16] A. H. MacDonald, Phys. Rev. B **29**, 6563 (1984).

[17] M. Y. Azbel, Zh. Eksp. Teor. Fiz. **46**, 929 (1964) [Sov. Phys. JETP **19**, 634 (1964)].

[18] G. H. Wannier, Phys. Status Solidi (b) **88**, 757 (1978).

[19] D. Hofstadter, Phys. Rev. B **14**, 2239 (1976).

[20] R. R. Gerhardts, D. Weiss, and U. Wulf, Phys. Rev. B **43**, 5192 (1991).

[21] M. A. Reed, J. N. Randall, R. J. Aggarwall, R. J. Matyi, T. M. Moore, and A. E. Westel, Phys. Rev. Lett. **60**, 535 (1988).

[22] K. Ismail, T. P. Smith, III, W. T. Masselink, and H. I. Smith, Appl. Phys. Lett. **75**, 2766 (1989).

[23] C. J. B. Ford, S. Washburn, R. Newbury, C. M. Knoedler, and J. M. Hong, Phys. Rev. B **43**, 7339 (1991).

[24] M. Büttiker, Phys. Rev. Lett. **57**, 1761 (1986).

[25] C. Barnes, B. L. Johnson, and G. Kirczenow (unpublished).

[26] This technique was utilized, for example, by J. T. Chalker and P. D. Coddington, J. Phys. C **21**, 2665 (1988).
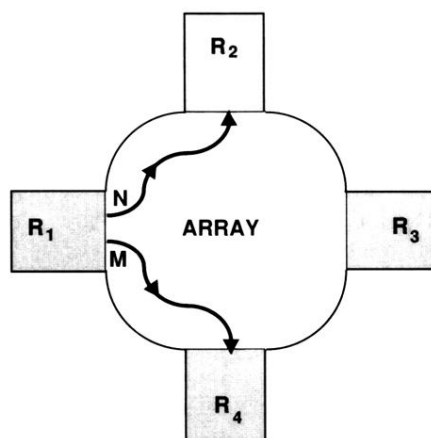
[27] G. Kirczenow, Surf. Sci. **263**, 330 (1991).

FIG. 1. Schematic of the quantum dot array attached to ideal reservoirs. The reservoirs are labeled $R1-R4$. N normal modes are populated by reservoir 1 and absorbed by reservoir 2, and M counterrotating modes are populated by $R1$ and absorbed at $R4$.
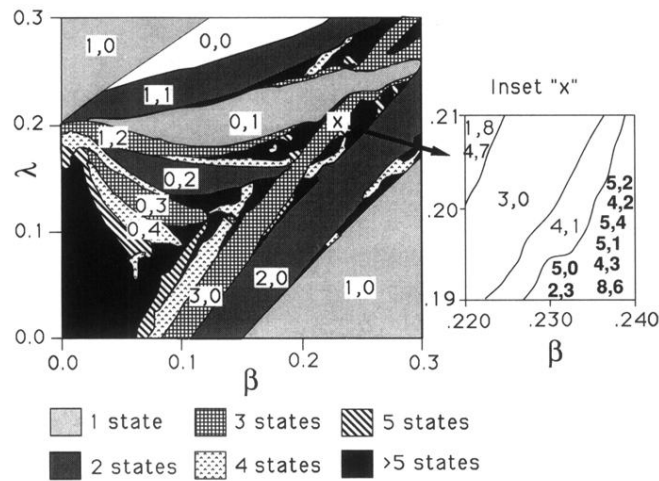
FIG. 3. The eigenspectra of a quantum dot strip with 90% transmission at the constrictions. Here $\lambda = -l$, the dot angular momentum; $\beta = Bd^2/\Phi_0$. The regions are marked according to the total number of propagating edge states as shown, and the labels indicate the number of normal and counterrotating states (N,M). The inset region "×" is enlarged, illustrating the complex region between 0,1 and 1,0 in the spectrum, where there is competition between numbers of rotating and counterrotating states. The labels are representative, and do not constitute all of the distinct regions present in the inset.